Sixth International Symposium on Turbulence and Shear Flow Phenomena
Seoul, Korea, 22-24 June 2009

IMPROVING COST-EFFECTIVENESS OF LES BY USING NON-REFLECTING BOUNDARY CONDITIONS: THE FLOW AROUND SIMPLIFIED ICE2 TRAIN

Branislav Basara
Advanced Simulation Technologies,
AVL LIST GMBH
Hans List Platz 1, 8020 Graz,
Austria
branislav.basara@avl.com

Siniša Krajnović
Department of Applied Mechanics,
Chalmers University of Technology
SE-41296 Gothenburg,
Sweden
sinisa@chalmers.se

Sergey M. Frolov
N. N. Semenov Institute of Chemical Physics,
Russian Academy of Sciences
Kosigin Street 4, 119991 Moscow,
Russia
sergey@frolovs.ru

ABSTRACT

The importance of having proper open or outflow boundary conditions for the calculation domain is a known issue in Computational Fluid Dynamics (CFD) for a long time and some recent developments were done originally without having Large Eddy Simulation (LES) applications in mind. An impact of it on LES results is even greater than in the case of some other modelling approaches due to the number of vortices which may pass through the outflow boundary. The flow may enter and leave the computational domain at the same time and at the same boundary. In such circumstances, it is important that numerical implementation of boundary conditions enforces certain physical constraints. This paper evaluates recently proposed non-reflecting boundary conditions on improving cost-effectiveness of LES calculations by reducing calculation domain and with that, also reducing the number of calculation cells which by the rule leads to a shorter computational time. The results will be shown for the flow around simplified ICE2 high-speed train subjected to a constant cross wind used in the previous work of Hemida and Krajnović (2009).

INTRODUCTION

The interest in using time-dependent simulations such as LES in vehicle aerodynamics has increased during last ten years as a result of success with LES simulations of flows around Ahmed body (Krajnović and Davidson, 2005a, 2005b) and some other external vehicle flows. However, most of these simulations were performed at Reynolds numbers that have lower power than real vehicle flows due to insufficient computer resources and required simulation time for real vehicle flows. There is ongoing research today in decreasing requirements for computational effort of LES by modelling the near wall flow rather than computing it. The objective of the present paper is to demonstrate how computational effort of LES can be decreased by shortening the computational domain and using outlet boundary conditions different from convective boundary conditions which have been a standard in LES of bluff body flows.

The largest interest in using time-dependent simulations in external vehicle aerodynamics is for flows that are inherently transient and very difficult to study using experimental facilities due to practical difficulties to obtain correct boundary conditions. An example of such situations is the flow around trains under the influence of cross winds. In the present paper we choose to demonstrate our approach on a flow around simplified ICE2 high-speed train subjected to a constant cross wind.

Despite a significant increase in computing power, there is almost always lack of computational cells when it comes to complex industrial applications. It is sometimes necessary to decrease the Reynolds-number as it was done in calculations presented here. However, and in this case, measurements of Orellano and Schober (2006) also show a very little influence of changing the Reynolds number on aerodynamic coefficients. They investigated three different

Reynolds numbers based on the height of the train and the free stream velocity: $1.074\text{x}10^6$, $1.79\text{x}10^6$, $2.5\text{x}10^6$. We have further decreased the Reynolds-number for almost one order compared to the measurements and it is equal to $2\text{x}10^5$. The computational mesh used for the standard run on the long domain was 12 million cells. In the work of Hemida and Krajnovic (2009), the mesh influence on the results was checked on 6 million cells in addition to that mesh of 12 million cells. The size of computational domains may influence the results as well. So almost as a rule, the length of the computational domain is taken to be between 20-30 heights behind the obstacle. For example, Sohankar et al. (1998) have shown that for the flow around a square cylinder, a distance of 26 widths of the cylinder are required between the cylinder and the outlet for low-Re number flows, while for the moderate Re-number, approximately 16 widths are sufficient if convective outlet boundary conditions are used.

A standard practice for the outflow boundary conditions is to use 'zero' gradient:

$$\frac{\partial U_i}{\partial x} = 0 \tag{1}$$

or so called 'convective' condition based on the free stream velocity components, thus

$$\frac{\partial U_i}{\partial t} + U_\infty \frac{\partial U_i}{\partial x} = 0 \tag{2}$$

This is probably the most popular variant of the outflow (or open) boundary conditions but nevertheless there is some reported influence of such boundary conditions to a zone approximately up to 10 heights upstream from the outflow boundary. This boundary condition was also used in LES calculations of Hemida and Krajnović (2009) on the longer domain having a distance between the train and the outflow boundary to be equal 21 heights, which is based on the experience and not on systematic studies of such geometries. Nevertheless, calculations are in a good agreement with the measurements.

The LES approach used in this paper is based on the sub-grid scale stress tensor modeled with the Smagorinski model, thus

$$\tau_{ij}^{SGS} = \tau_{ij} - \frac{1}{3}\tau_{kk} = -2\nu_{SGS}S_{ij} \tag{3}$$

where the sub-grid scale viscosity is written as

$$\nu_{SGS} = \left(C_s f \Delta\right)^2 |S| \tag{4}$$

and the value $C_s = 0.1$, while the resolved rate-of-strain tensor is $|S| = \left(2S_{ij}S_{ij}\right)^{1/2}$. The filter width Δ is taken as the cubic root of the volume of a computational cell.

NUMERICAL PROCEDURE

The available space will not permit all details but just crucial elements related to the numerical procedure and the non-reflecting boundary conditions to be explained here.

For this work, the non-reflecting boundary condition is implemented into the commercial CFD package AVL FIRE (FIRE Manual, 2008). This boundary condition is well tested in conjunction with URANS methods as shown by Frolov et al. (2006, 2009) and Basara et al. (2007).

AVL FIRE code employs the finite volume discretization method, which rests on the integral form of the general conservation law applied to the polyhedral control volumes. All dependent variables, such as momentum, pressure, density, turbulence kinetic energy, dissipation rate, and passive scalar are evaluated at the cell center. The cell-face based connectivity and interpolation practices for gradients and cell-face values are introduced to accommodate an arbitrary number of cell faces. A second-order midpoint rule is used for integral approximation and a second order linear approximation for any value at the cell-face. The convection is solved by a variety of differencing schemes (upwind, central differencing, MINMOD, and SMART). The rate of change is discretized by using implicit schemes, namely Euler implicit scheme and three time level implicit scheme of second order accuracy. The overall solution procedure is iterative and is based on the Semi-Implicit Method for Pressure-Linked Equations algorithm (SIMPLE). For the solution of a linear system of equations, a conjugate gradient type of solver and algebraic multi-grid are used.

Therefore, the boundaries presented here are adjusted to the discretization method adopted for the polyhedral cell type. For a grid cell P with the volume V surrounded by it's neighbors P_j, the discretized control volume equation can be written as:

$$\frac{d}{dt}\left(\rho_P V_P \phi_P\right) + \sum_{j=1}^{n_f} C_j - \sum_{j=1}^{n_f} D_j = (sor_\phi^V)_P V_P + \sum_{j=1}^{n_f}\left(sor_{\phi k}^A S_k\right)_j \tag{5}$$

where C_j and D_j are convective and diffusion transport through the face j, respectively; n_f is the number of cell-faces, and sor^V and sor^A terms are volumetric and surface sources respectively.

With the use of linear interpolation, the cell face values can be calculated as

$$\phi_j = f_j\phi_p + (1-f_j)\phi_{p_j} \tag{6}$$

where f_j is the cell face interpolation factor. In the case that the vector connecting two centers P and P_j does not pass through the face center, an additional correction may be introduced as suggested by Demirdzic and Muzaferija (1995). The cell gradients can be calculated by using either the Gauss' theorem,

$$\nabla\phi_p = \frac{1}{V_p}\sum_{j=1}^{n_f}\phi_j s_j \tag{7}$$

or a linear least-square approach e.g. Muzaferija (1994). Using Gauss' theorem and with the simple mathematical reconstructions to replace vertex values only with the contributions from cells P and P_j, one can arrive at the following formula for the cell face gradient, thus

$$\nabla\phi_j = \overline{\nabla\phi}_j + \frac{s_j}{s_j \cdot d_j}\left[\left(\phi_{Pj} - \phi_P\right) - \overline{\nabla\phi}_j \cdot s_j\right] \tag{8}$$

where

$$\overline{\nabla\phi_j} = f_j\nabla\phi_j + (1-f_j)\nabla\phi_j \tag{9}$$

where s_j is the surface vector and d_j is the distance vector between two points.

Using Equation (8) for cell face gradients, the diffusion term can be written as

$$D_j = \underbrace{\overline{\Gamma}_{\phi j}\frac{s_j^2}{s_j \cdot s_j}\left(\phi_{Pj}-\phi_P\right)}_{normal-diffusion} + \underbrace{\overline{\Gamma}_{\phi j}\overline{\nabla\phi}_j\left(s_j-\frac{s_j^2}{s_j\cdot d_j}d_j\right)}_{cross-diffusion} \quad (10)$$

The cross-diffusion part of Equation (13), which vanishes on the orthogonal grid, is treated in a deferred correction manner and introduced in discretized equations as surface source term. A deferred correction approach is also used for the treatment of convection fluxes, thus

$$C_j = \dot{m}_j\phi_j^{UDS} + \underline{\gamma_\phi\left|\dot{m}_j\right|\varphi_j\left(\phi_{P_j}-\phi_P\right)} \quad (11)$$

where $\dot{m}_j$ is the mass flux, and γ_ϕ is the blending factor between UDS and higher order scheme $0 \le \gamma \le 1$. The underlined term is calculated by using values from the previous iteration step. The flux limiter φ_j is provided by the higher order differencing scheme used to ensure a bounded solution. The convection and diffusion fluxes on the boundaries are calculated the same as for the internal faces.

Derivation of the local non-reflecting boundary conditions at the open boundary is based on finding the solution of linearized Euler equations vanishing at infinity for both incompressible and compressible formulations. Based on that, Frolov et al. (2001, 2006) derived more accurate non-reflecting boundary conditions for incompressible flow which are given in the form:

$$\frac{\partial U_i}{\partial t} + U_\infty\frac{\partial U_i}{\partial x} = -L\Psi \quad (12)$$

$$\frac{\partial P}{\partial x} = -LP \quad (13)$$

Let us assume that a discretization of operator L is the matrix A which has eigenvalues λ_i and corresponding eigenvectors e_i. Matrix A is the approximation of the two-dimensional Laplace operator in the plane, e.g. (y,z), thus

$$\Delta_{yz} = \frac{\partial^2}{\partial y^2}+\frac{\partial^2}{\partial z^2} \quad (14)$$

In the frame of the control volume dicretization which is the basis of FIRE, we could write for the orthogonal mesh next to the boundary as (so no cross diffusion term, for details of discretization see above and also Basara, 2004).

$$\Delta\Phi = \int_S grad\Phi\cdot d\vec{s} \approx \sum_{j=1}^{n_f}\left(\Phi_{P_j}-\Phi_P\right)\frac{s_j\cdot s_j}{d_j\cdot s_j} \quad (15)$$

Following $\Delta\Phi=0$ we can get the elements of the matrix A from following equation

$$\Phi_P a_P = \sum_{j=1}^{n_f}\Phi_{P_j}a_{P_j} \quad (16)$$

where $a_P = \sum_{j=1}^{n_f}a_{P_j}$.

Furthermore, the matrix $S=(e_{ij})$ transforms the matrix A to the diagonal form:

$$S^{-1}AS = D^0 \quad (17)$$

leading the matrix B which corresponds to the operator L^{-1} to be equal

$$B = S\sqrt{D^0}S^{-1} \quad (18)$$

where D^0 is the diagonal matrix with $d_{ii}^0 = \lambda_i$. Or the elements $b_{i,j}$ of the matrix B can be obtained from

$$b_{i,j} = \sum_{k=1}^{n} e_{i,k}d_{k,k}e_{k,j} \quad (19)$$

where elements of diagonal matrix D is given as

$$d_{k,k} = \frac{1}{\sqrt{\lambda_k}} \quad (20)$$

Note that the matrix A is constructed only once at the beginning of calculation. For more details of derivations, see original references of Frolov et. al (2001, 2009). The size of matrix A is the square of total number of cells next to the non-reflecting boundary. For large cases, this can require a large memory as well but also a longer computing time. However, preliminary results on simple benchmarks (Basara, 2007, and Frolov et al., 2009) showed that this non-reflecting boundary conditions provides very accurate results even placed very near to separating regions, or to regions with strong pressure gradients, etc.

In the case when the non-reflecting boundary conditions is employed, the original domain shown in Figure 1 was reduced so that the length between the train and the outlet was decreased by the factor of 2. Furthermore, the mesh had to be modified in order to reduce a number of cells at the non-reflecting boundary (the size at the outlet was approximately reduced on the size of 400x400 cells). The total number of computational cells for the shorter domain was about 7,5 million cells.

In this work, Equation (12) was not used to update velocity but rather velocities were updated the same as for the pressure boundary and the SIMPLE algorithm (Basara, 2003) but this time having pressure from Equation (13) as the 'new' pressure at the boundary, thus

$$\frac{\partial U_i}{\partial x} = -f\left[\left(\frac{\partial P}{\partial x}\right)^{new}-\left(\frac{\partial P}{\partial x}\right)^{old}\right] \quad (21)$$

The function f in Equation (21) depends from the interpolation practices and from the pressure boundary implementation in the numerical procedure (see also Ferziger and Peric, 1996). For the implementation in FIRE, the following discretized equation is solved:

$$U_{n,b} = U_{n,P} - \left(\frac{V_P}{a_P}\right)\frac{s_{n,b}}{s_b\cdot d_b}\left[\left(P_b-P_P\right)-\nabla P_P\cdot d_b\right] \quad (22)$$

where n=1,2,3 (for each velocity component). This turns to be a more robust solution than to calculate velocities from Equation (12) probably due to relatively large turbulence being transported through the boundary. The velocity correction as a part of SIMPLE algorithm at the boundary can be approximated as

$$U_{n,b}^{'} \approx -\left(\frac{V_P}{a_P}\right)\frac{s_{n,b}}{s_b\cdot d_b}\left(P_b^{'}-P_P^{'}\right) \quad (23)$$

where the pressure boundary correction is set to zero. This is used as a Dirichlet boundary condition in the pressure correction equation.

RESULTS AND DISCUSSION

LES is used to calculate the flow around a simplified ICE2 train (the scale is 1:10) under side wind conditions at 30^o yaw angle. Therefore, the computational model of the train is yawed 30^o to the free-stream direction as shown in Figure 1. The simplified train model consists of a leading car and attached end car dummy. The total length of the train is L=3.552m and the height D=0.358m. The clearance between the train and the floor is 0.15D. The physical time step is Δt = 0.0001seconds which gives a maximum Courant-Friedrichs-Levy CFL number of about 1.5

In calculations of Hemida and Krajnović (2009), the minimum distance between the train tail and the exit of the computational domain is 21D. In the second case with employed non-reflecting boundary conditions, this distance was reduced to 10D. An O-type mesh was made around the train model. The computation mesh for the short domain calculation is obtained by cutting the original mesh after 10D behind the train modifying the exit part by the employment of an arbitrary interface in order to reduce the number of cells next to the outlet boundary. Therefore, the computational cells are unchanged in the most of computational domain.

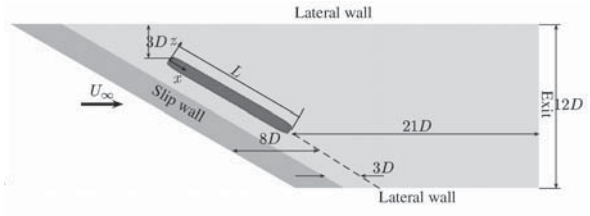

Figure 1: Computational domain from Hemida and Krajnović (2009) (note that the distance between the train and the exit in the original and the shorter domain was 21D and 10D, respectively).

The flow enters the computational domain with a uniform velocity profile constant in time. Since the inlet boundary condition is a uniform, the distance between the inlet plane and the train is long enough not to influence results on the train. This distance was kept the same for the shorter domain as well. For the long domain, a convective boundary condition is employed at the domain exit while a non-reflecting boundary condition is used at the exit of the short domain. A slip boundary condition is applied on a part extending 5D from the inlet plane as shown in Figure 1 to suppress the development of a boundary layer, while a no-slip boundary condition is used for the rest of the floor.

The surface pressure distributions are compared with the measurements of Wu (2004) at certain cross sections. Comparisons of the pressure coefficient values from LES with the experimental data at positions marked in Figure 2a, are presented in Figures 2(b-d) and 3(a-c). The agreement between LES results and the experimental values is very good at all sides of the train except on the under-body at positions of the bogies which were present in the experiments but omitted in the simulations. In this paper, we look more for differences between the long and the short domain rather than in the absolute difference from the measured values.

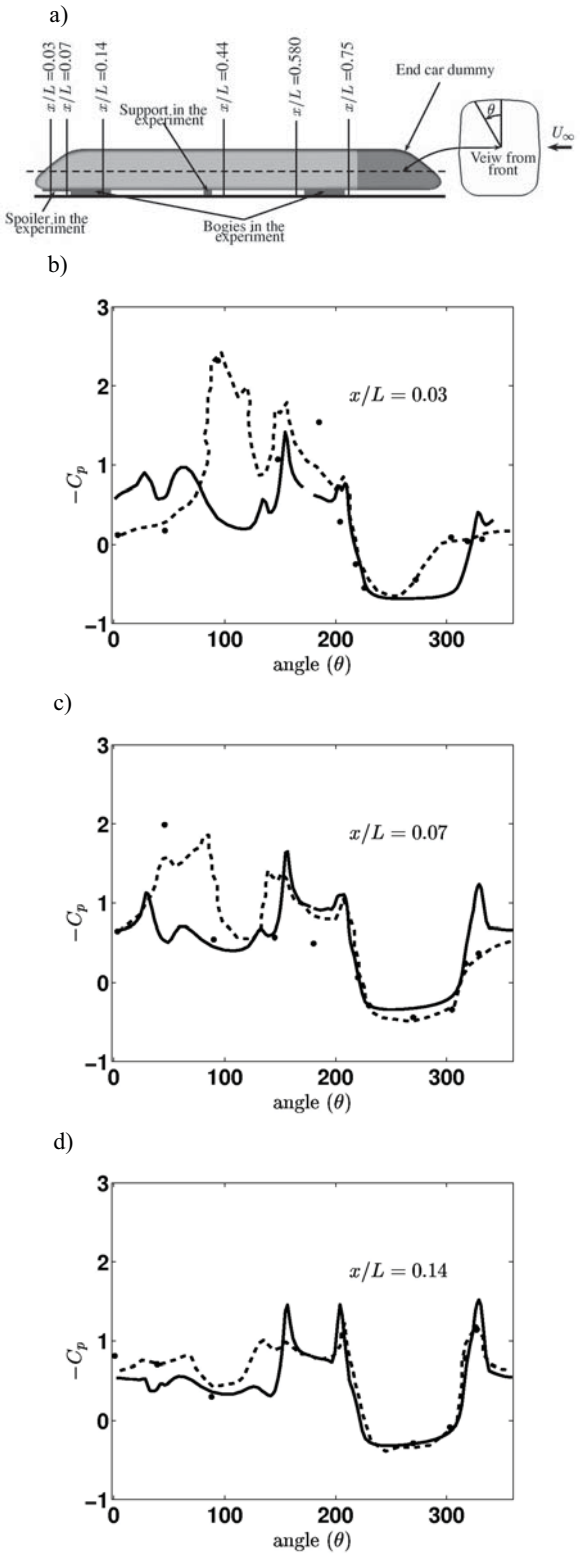

Figure 2: Comparison of the surface pressure coefficient distribution along the length of the train at the distance x/L=0.03 (b), 0.07 (c), 0.14 (d): Short domain (solid line); Long domain from Hemida and Krajnović (2009) (dashed line); experimental data from Wu (2004) (symbols). Figure (a) shows the location of the measured time-averaged pressure distributions and the orientation of angle Θ.

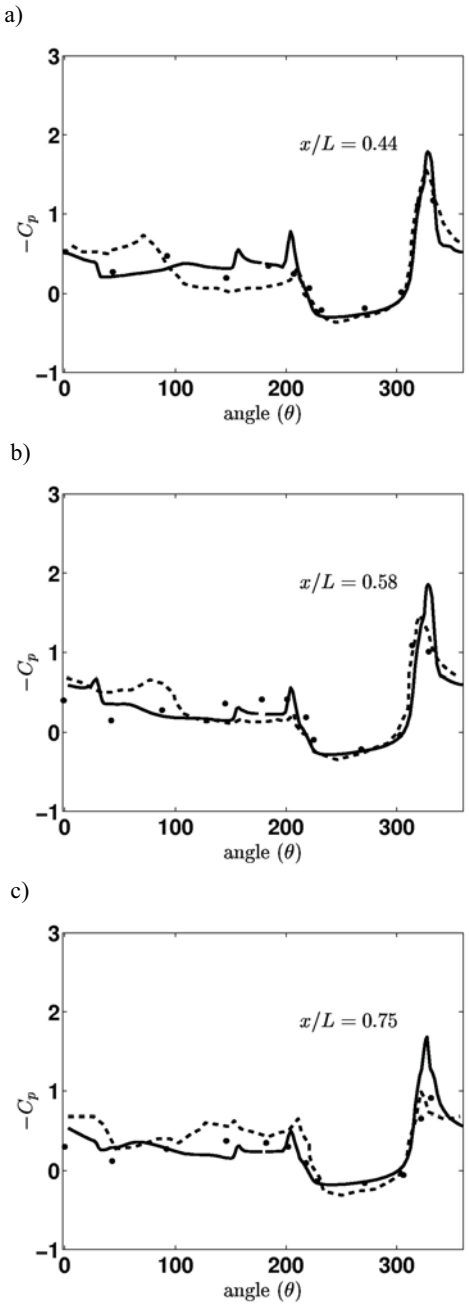

Figure 3: Comparison of the surface pressure coefficient distribution along the length of the train at the distance x/L=0.44 (a), 0.58 (b), 0.75 (c): Short domain (solid line); Long domain from Hemida and Krajnović (2009) (dashed line); experimental data from Wu (2004) (symbols).

The first two profiles show some differences at the nose of the train (x/L<0.14) but the rest of results are very similar and close to the measurements. Those differences between results for different domains could be probably due to different time intervals used for averaging results.

Note also that the computational mesh was not completely identical in the cut part of longer domain and in the short domain due to reduction of a number of cells at the non-reflecting boundary. Far from the nose of the train, the results for different domains are very close to each other and to measurements as well.

The agreement of the results from both LES (with the short and the long domain) with the experimental data is good despite the seven times lower Renolds number in the LES compared to experiments. For the analysis of all results in detail and the Reynolds number effects, see Hemida and Krajnović (2009).

Figure 4 shows the time averaged LES streamlines projected on the train surface. From the figure, it is clear that the time-averaged surface flow patterns are very similar for the long and short domains. Especially there is a good agreement on the streamwise face where the flow is moving toward the roof and the bottom of the train as well as on the leeward side of the train. Some discrepancies are present in the calculations on the flow separation on the upper-side and bottom-side face but differences are relatively small and could be attributed to differences in averaging times between the two LES.

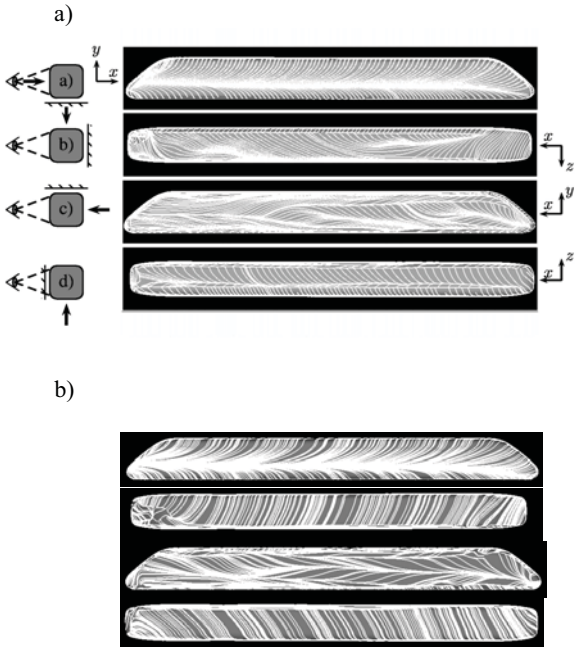

Figure 4: Comparison of the time-averaged trace lines projected on the surface of the train: (a) Long domain from Hemida and Krajnović (2009); (b) Short domain.

Figure 5 shows the wake structures by means of the instantaneous pressure. In both cases, very similar observations can be made (again note that the time step is different). The flow separates from the top-side face at the windward edge but stays attached to the bottom side face before entering the wake. The first upper vortex stretches in the wake flow from the nose tip (see the notation in Figure 5). This vortex breaks up on about 5D from its onset in both of the cases. Hemide and Krajnović (2009) showed that the vortex shedding in the wake mainly comes from the lower vortices which are highly unsteady. The same conclusions

can be drawn out from calculations of longer and shorter domains.

Comparing all results and analysing flow filed for the shorter domain, there is no evidence that the non-reflecting boundary placed at the distance of 10D from the train will influence calculations to a larger extent.

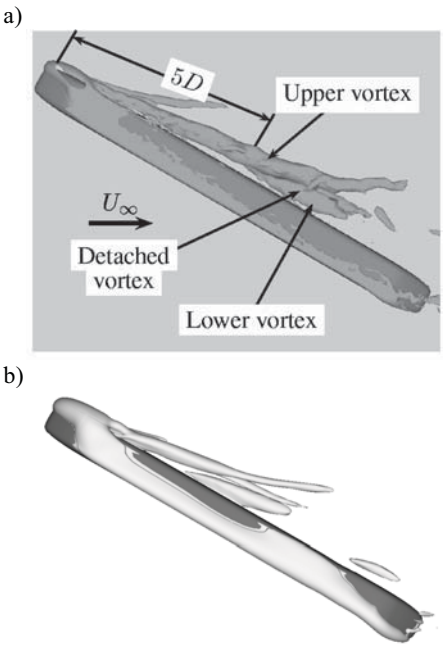

Figure 5: Isosurface of the instantaneous pressure p=-0.4 Pa: a) Long domain from Hemida and Krajnović (2009). b) Short domain. View is from above the train.

CONCLUSIONS

The results obtained for two different lengths of the calculation domain show that the employment of the non-reflecting boundary conditions could improve cost-effectiveness of LES as the number of computational cells can be decreased for up to 40% or even more cells, e.g. a reduction of a computing time or reduction on number of computer processors as with less processors smaller computational cases still can be calculated. A total reduction with and without non-reflecting boundaries will depend also on the type of meshing e.g. the block structured or the mesh with the local grid refinement, etc. The modification of originally proposed non-reflecting boundary conditions related to the update of velocity, which is now re-calculated as for the standard pressure boundary condition, provides very robust calculations. The future study will include meshes with the local grid refinement and further shortening of the computational domain.

REFERENCES

AVL FIRE Manual v2008, 2008, Advanced Simulation Technologies, AVL List GmbH, Graz, Austria.

Basara, B., 2004, "Employment of the Second-Moment Turbulence Closure on Arbitrary Unstructured Grids", *International Journal for Numerical Methods in Fluids*, Vol. 44, pp. 377-407.

Basara, B., 2003, "Basic Boundary Conditions for Incompressible and Compressible flows using Unstructured Meshes", *ASME paper FEDSM2003*.

Basara, B., Frolov, S. M., Lidskii, B., and Posvyanskii V. S., 2007, "Evaluation of General Non-Reflecting Boundary Condtions for Industrial CFD Applications ", *APS-DFD Annual meeting,* Salt Lake City, USA.

Demirdzic, I., and Muzaferija, S., 1995, "Numerical Method for Coupled Fluid Flow, Heat Transfer and Stress Analysis Using Unstructured Moving Meshes and Cells of Arbitrary Topology ", *Comp. Methods Appl. Mech. Eng s*, Vol. 125, pp. 235-255.

Ferziger, J. H., and Peric, M., 1996, "Computational Methods for Fluid Dynamics", Springer, Berlin, Germany.

Frolov, S. M., Basevich, V. Ya., Belyaev, A. A., Posvyanskii V. S., and Radvogin, Yu, B., 2001, "Modeling of Confined Flame Stabilization by Bluff Bodies ", *Advances in Chemical Propulsion: Science to Technology,* G.D. Roy, ed., CRC Press, Washington, D.C., Vol. 12, pp. 191-214.

Frolov, S. M., 2006, "Development and Implementation of Non-Reflecting Boundary Condition ", *Technical Report AVL-159190*, Semenov Institute of Chemical Physics, Moscow, Russia.

Frolov, S. M., Lidskii, B., Posvyanskii V. S., and Basara, B., 2009, " General Non-Reflecting Boundary Conditions for Incompressible and Compressible Flows", *in preparation.*

Hemida, H., and Krajnović, S., 2009, "Exploring Flow Structures Around a Simplified ICE2 Train Subjected to a 30 Degree Side Wind Using Large-Eddy", *J. of Engineering Applications of Computational Fluid Mechanics,* Vol. 3, pp. 28-41.

Krajnović, S. and Davidson, L., 2005a, "Flow Around a Simplified Car, Part 1: Large Eddy Simulation", *ASME: J. of Fluids Engineering,* Vol. 127, pp. 907-918.

Krajnović, S. and Davidson, L., 2005b, "Flow Around a Simplified Car, Part 2: Understanding the Flow", *ASME: J. of Fluids Engineering,* Vol. 127, pp. 919-928.

Muzaferija, S., 1994, "Adaptive Finite Volume Method for Flow Predictions Using Unstructured Meshes and Multigrid Approach", *PhD Thesis*, Imperial College, University of London, UK.

Orellano, A., and Schober, M., 2006, "Aerodynamic Performance of a Typical High-Speed Train", *WSEA Transactions on Fluid Mechanics*, Vol. 1, pp. 1790-5087. Iowa State Univ., Ames, IA.

Sohankar, A., Norberg, C., and Davidson, L., 1998, "Low-Reynolds Number Flow Around a Square Cylinder at Incidence: Study of Blockage, Onset of Vortex Shedding and Outlet Boundary Condition", *Int. J. for Numerical Methods in Fluids,* Vol. 26, pp. 39- 56.

Wu, D., 2004, "Predictive Prospects of Unsteady Detached-Eddy Simulations in Industrial External Aerodynamics Simulations", *Diploma Thesis,* Matriculation number: 219949, Lehstruhl fur Strömungslehre und Aerodynamishes Institute, Aachen, Germany.